

Article

# The Shape-Memory Effect of Hindered Phenol (AO-80)/Acrylic Rubber (ACM) Composites with Tunable Transition Temperature

Shi-kai Hu <sup>1,2</sup>, Si Chen <sup>1</sup>, Xiu-ying Zhao <sup>1,\*</sup>, Ming-ming Guo <sup>1,2</sup> and Li-qun Zhang <sup>1</sup>

<sup>1</sup> Key Laboratory of Beijing City on Preparation and Processing of Novel Polymer Materials, Beijing University of Chemical Technology, Beijing 100029, China; 2017400073@mail.buct.edu.cn (S.-k.H.); aircs123@163.com (S.C.); guomm57@swu.edu.cn (M.-m.G.); zhanglq@mail.buct.edu.cn (L.-q.Z.)

<sup>2</sup> SINOPEC Beijing Research Institute of Chemical Industry, Beijing 100013, China

\* Correspondence: zhaoxy@mail.buct.edu.cn; Tel.: +86-10-6443-4860

Received: 31 October 2018; Accepted: 26 November 2018; Published: 4 December 2018



**Abstract:** To broaden the types and scope of use of shape-memory polymers (SMPs), we added the hindered phenol 3,9-bis[1,1-dimethyl-2-[b-(3-tert-butyl-4-hydroxy-5-methylphenyl)propionyloxy]ethyl]-2,4,8,10-tetraoxaspiro-[5,5]-undecane (AO-80), which comprises small organic molecules, to acrylic rubber (ACM) to form a series of AO-80/ACM rubber composites. The structural, thermal, mechanical property, and shape-memory properties of the AO-80/ACM rubber composites were investigated. We identified the formation of intra-molecular hydrogen bonding between –OH of AO-80 and the carbonyl groups and the ether groups of ACM molecules. The amount of AO-80 used can be adjusted to tailor the transition temperature. AO-80/ACM rubber composites showed excellent shape recovery and fixity. The approach for adjusting the transition temperature of AO-80/ACM rubber composites provides remarkable ideas for the design and preparation of new SMPs.

**Keywords:** acrylic rubber; shape-memory polymer; hindered phenol; hydrogen bonding

## 1. Introduction

Shape-memory materials (SMMs) can change from one pre-determined shape to another in response to a certain stimulus [1,2]. Research on shape-memory polymers (SMPs) can be fundamental and applied. SMPs possess many advantages over their well-investigated metallic counterparts, shape-memory alloys; these advantages include excellent processability, light weight, and notable flexibility in terms of material design [3–5]; SMP applications include medical devices, actuators, sensors, artificial muscles, switches, smart textiles, and self-deployable structures [4–7]. SMPs can return into an original shape upon the application of stimuli, such as temperature [8–10], humidity [11,12], light [13–16], electricity [8,17–20], pH [15,21–24], and irradiation. This memory phenomenon is because a polymer network has reversible and fixed phases. The reversible phases can be shaped under certain conditions. Reversible phases use ionic bond [1,25], vitrification [25,26], reversible crystallization [27], hydrogen bond [28,29], or supramolecular interactions [30,31] to maintain this metastable shape until an activation energy is used to facilitate a return to the original shape. The fixed phases allow deformation but hold the relative location of the chains. Fixed phases include physical and covalent cross-links, such as crystalline or glassy domains in polymers, or supramolecular interactions [32]. For thermally induced SMPs, when the deformation of SMP is above its switch transition temperature ( $T_{trans}$ ) and then cooled below  $T_{trans}$ , most internal stress can be stored in cross-linking structure; by heating the SMP above its  $T_{trans}$ , the SMP recovers its original shape by releasing the internal stress [33,34]. When reheated above  $T_{trans}$  without stress, the cross-linking phase assumes its permanent shape.  $T_{trans}$  can either be the glass transition

temperature ( $T_g$ ) or melting temperature ( $T_m$ ) of polymers. In general, the temperature province of  $T_{trans}$  of current SMMs reaches above room temperature. However, in specific conditions, such as deep-sea and polar region explorations,  $T_{trans}$  of SMMs should be lower than room temperature and can be adjusted and controlled by specific methods. A critical parameter for SMPs lies in its shape memory  $T_{trans}$ . For an amorphous SMP polymer, it is important to develop new methods to tailor its  $T_g$ , which corresponds to its shape memory  $T_{trans}$ . Zhao et al. created a nano- or molecule-scale-hindered phenol and polar rubber compound. Their research indicated that  $T_g$  of the developed material could be tailored by changing the kind and dosage of small organic molecule-hindered phenol [35,36]. This phenomenon was attributed to hydrogen bonding between hindered phenol 3,9-bis[1,1-dimethyl-2-[b-(3-tert-butyl-4-hydroxy-5-methylphenyl)propionyloxy]ethyl]-2,4,8,10-tetraoxaspiro-[5,5]-undecane (AO-80) and polar rubber. Such interactions will result in the molecular-level dispersion of AO-80 in CPE and rubber matrix and enhancement of intermolecular friction, which will further increase  $T_g$ . It is well known that typical epoxy-based materials which have been applied extensively in coatings, adhesives, and matrix material for structural composites are rigid with relatively low failure strains. There are many references regarding shape-memory epoxy composites that all have good shape memory with a high shape fixity ( $R_f$ ) ratio and high shape recovery ratio ( $R_r$ ), but these composites all have a short elongation at break [37–42]. In this study, AO-80 had been studied to prepare AO-80/acrylic rubber (ACM) nanocomposites with high failure strains compared to shape-memory epoxy composites. The structure of AO-80 is shown in Figure 1. AO-80/ACM rubber nanocomposites possibly possess remarkable filler/matrix interfacial properties because the AO-80 molecule features numerous polar functional groups (hydroxyl and carbonyl) that can form strong intermolecular interactions with ACM. An elastomer will exhibit shape-memory functionality when the material can be stabilized in the deformed state in a temperature range that is relevant for particular applications. Similar to normal polymers, SMPs also possess 3D molecular network-like architectures. ACM can exhibit 3D network structures after crosslinking. These cross-linked structures ensure that the polymer can maintain a stable shape at the macroscopic level by enabling the original and recovered shapes. This system also features a  $T_g$  below the room temperature, and temperature can be adjusted and controlled within a particular scope by incorporating small organic molecules to increase  $T_g$  [35,36], which will broaden the kind and scope of use of SMPs. In this study, we designed a series of AO-80/ACM rubber composites with high failure strains, the  $T_{trans}$  of which can be tailored by adding a dosage of small organic molecule-hindered phenol. No study or similar work has investigated the shape-memory effect of AO-80/ACM rubber composites, thereby broadening the list of SMPs with excellent shape-memory properties.

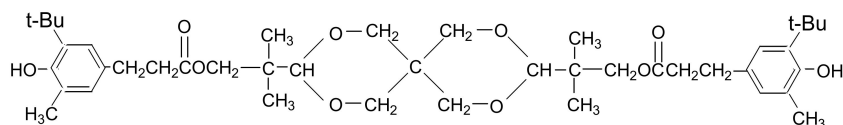


**Figure 1.** Chemical structure of hindered phenol 3,9-bis[1,1-dimethyl-2-[b-(3-tert-butyl-4-hydroxy-5-methylphenyl)propionyloxy]ethyl]-2,4,8,10-tetraoxaspiro-[5,5]-undecane (AO-80).

## 2. Materials and Methods

### 2.1. Materials

ACM (AR-801) was provided by Tohpe Corp (Sakai, Japan). AO-80 was obtained from Asahi Denka (Tokyo, Japan). Other ingredients and chemicals were obtained from China and were used as received.

### 2.2. Sample Preparations

AO-80/ACM rubber composites were obtained as follows: (1) After ACM was kneaded for 3 min, AO-80 (without previous treatment) was added into ACM. (2) After these mixtures were kneaded

for 5 min, the AO-80/ACM mixtures were blended with compounding and crosslinking additives, including 5.0 phr of zinc oxide (CAS No: 1314-13-2), 1.0 phr of stearic acid (CAS No: 57-11-4), 0.5 phr of potassium stearate (CAS No: 593-29-3), 4 phr of sodium stearate (CAS No: 822-16-2), and 0.5 phr of sulfur (CAS No: 7704-34-9). The mixtures were then kneaded for 10 min. The mixtures of AO-80/ACM were kept for at least 24 h. (3) Finally, the mixtures of AO-80/ACM were set at 180 °C and 15 MPa for 20 min and then naturally cooled down to prepare AO-80/ACM rubber composites.

### 2.3. Methods

The structure, shape-memory properties, and mechanical and thermal properties of AO-80/ACM rubber composites were systematically evaluated by differential scanning calorimetry (DSC), dynamic mechanical analysis (DMA), and Fourier-transform infrared (FT-IR) spectroscopy. The DSC curves were acquired from −60 °C to 150 °C at a rate of 10 °C/min with a STAR<sup>e</sup> system calorimeter (Mettler–Toledo Co., Zurich, Switzerland). FT-IR spectra were acquired by using a Spectra-Tech ATR attachment to scan the samples.

The static mechanical properties of AO-80/ACM rubber composites were determined according to ASTM D638 by using a CMT4104 Electrical Tensile Tester (SANS Testing Machine Co., ShenZhen, China) at a rate of 500 mm/min at room temperature. The strip dimensions for testing were 20 mm in length, 6 mm in width, and 2 mm in thickness. Hardness was tested according to ASTM D2240-2015.

The shape-memory effect analysis of AO-80/ACM rubber composites was investigated on the DMA Q800 (TA Instruments, New Castle, DE, USA) using controlled-force mode with rectangular samples (6 mm in width and 2 mm in thickness). Prior to the investigation, the temperature was adjusted to an equilibration at  $T_{trans} + 20$  °C for 10 min. In step 1 (deformation), the sample was stretched to a designed value ( $\varepsilon = 55\%$ ,  $\varepsilon = 100\%$ ,  $\varepsilon = 130\%$ ) by ramping the force from a preload value of 0.005 N at a rate of 0.5 N/min. In step 2 (cooling), the specimen was cooled to fix the deformed sample under constant force at the rate of 3 °C/min to  $T_{trans} - 20$  °C. In step 3 (unloading and fixing), the force of the specimen was unloaded at a rate of 0.5 N/min to a preload value (0.005 N). Then, an equilibration at  $T_{trans} - 20$  °C for 10 min to ensure shape fixing was performed. In the final step (recovery), the specimen was reheated to  $T_{trans} + 60$  °C at the rate of 3 °C/min [37]. All experiments were carried out three times successively and the average results between second and third cycles are shown in the paper. From the curves, the shape recovery ratio ( $R_r$ ) and the shape fixity ratio ( $R_f$ ) for the shape-memory effect were computed as follows:

$$\text{Shape recovery : } R_r(N) = \frac{\varepsilon_m - \varepsilon_p(N)}{\varepsilon_m - \varepsilon_p(N-1)} \times 100\% \quad (1)$$

$$\text{Shape fixity : } R_f(N) = \frac{\varepsilon_u(N)}{\varepsilon_m(N)} \times 100\% \quad (2)$$

where  $\varepsilon_m$ ,  $\varepsilon_u$  and  $\varepsilon_p$  are strains after the step of cooling, unloading, and recovery process, respectively.  $N$  refers to a consecutive number in a cyclic shape-memory measurement.

Dynamic mechanical properties were investigated on a DMA (Rheometric Scientific Co., Piscataway, NJ, USA). The strip dimensions for testing were 20 mm in length, 6 mm in width, and 2 mm in thickness. The curves of  $E'$ - $T$  were acquired from −60 °C to 150 °C at a rate of 3 °C/min and with a frequency of 1 Hz at an amplitude of  $\varepsilon = 0.3\%$ .

Shape recovery observations of the AO-80/ACM rubber composites were carried out in water. The composites were cut into rectangular strips with dimensions of 100.0 mm × 10.0 mm × 2.0 mm. The rectangular strips were fixed in a temporary shape at  $T_{high}$  and then cooled down to  $T_{low}$ . The rectangular strips in temporary shape were placed in a water bath at  $T_{high}$  while recording images of shape recovery using a video camera at a rate of 20 frames/s. Among the aforementioned procedure/conditions,  $T_{high}$  was equal to  $T_{trans} + 20$  °C, and  $T_{low}$  was equal to  $T_{trans} - 20$  °C.

### 3. Results

#### 3.1. $T_g$ of AO-80/ACM Rubber Composites

Figure 2 shows that the neat ACM featured a  $T_g$  of approximately  $-11\text{ }^\circ\text{C}$ . Compared with the neat ACM, AO-80/ACM composites showed a  $T_g$  between those of neat ACM and quenched AO-80(40.9) [36].  $T_g$  of AO-80/ACM rubber composites shifted from  $-11\text{ }^\circ\text{C}$  to  $10\text{ }^\circ\text{C}$  when the dosage of AO-80 was added from zero phr to one hundred phr. The DSC curves of the composites showed neither  $T_g$  peak nor melting of AO-80 [36,43], which suggest that dispersion of AO-80 in ACM was at the molecular level by blending, and AO-80/ACM rubber composites were successfully prepared as expected. Strong intermolecular interactions were formed between AO-80 molecules and polar functional groups (ester and ether groups) of ACM. Hydrogen bonding between ACM and AO-80 are analyzed later. With both polar molecules, intermolecular interactions significantly hindered the slide of ACM chain and increased  $T_g$  of ACM composites.

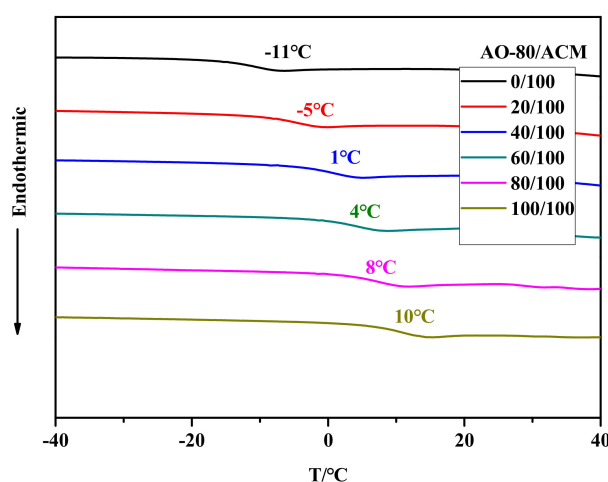


**Figure 2.** DSC curves of AO-80/acrylic rubber (ACM) rubber composites.

#### 3.2. FT-IR of AO-80/ACM Rubber Composites

Interactions between different functional groups can be investigated through molecular dynamics simulation and FT-IR [44,45]. Figure 3 shows the FT-IR/ATR spectra of neat ACM and AO-80/ACM rubber composites. Figure 3a shows that the FT-IR/ATR spectra of all AO-80/ACM rubber composites indicate significantly wide peaks at  $1135\text{ cm}^{-1}$  to  $1195\text{ cm}^{-1}$ , which were assigned to C-O-C bending vibration and symmetric and antisymmetric stretching vibrations. The peak position gradually shifted to a higher wave number from  $1158.5\text{ cm}^{-1}$  to  $1163\text{ cm}^{-1}$  when the dosage of AO-80 was added from zero phr to one hundred phr, determining that -O- of C-O-C can bond with -OH of AO-80. Figure 3b shows the composition dependence of FT-IR spectra for the  $\text{-C=O}$  stretching regions of AO-80/ACM rubber composites. As AO-80 content increased, the  $\text{-C=O}$  peak position shifted to a higher wave number from  $1730.0\text{ cm}^{-1}$  to  $1732.0\text{ cm}^{-1}$  when the dosage of AO-80 was added from zero phr to one hundred phr. Studies reported that hydrogen-bonded vibration will present a frequency shift [35,36]. Figure 3c shows the  $\text{-OH}$  stretching regions of AO-80/ACM rubber composites. The position of  $\text{-OH}$  peak shifted to a lower wave number from  $3555.1\text{ cm}^{-1}$  to  $3498.7\text{ cm}^{-1}$  when the dosage of AO-80 was added from zero phr to one hundred phr. The hydrogen bonding between carbonyl and ether groups of segments of ACM and -OH groups of AO-80 was observed. The total frequency shift as a measure of the strength of hydrogen bonding is generally accepted [46–48]. Thus, these results indicate that as the dosage of AO-80 increased, the strength of the hydrogen bonding among functional groups between ACM and AO-80 improved. The result corroborates that the  $T_g$  of AO-80/ACM rubber composites increased with the dosage of AO-80, increasing because of hydrogen bonding. Figure 4 shows the possible hydrogen bonding of AO-80/ACM rubber composites.

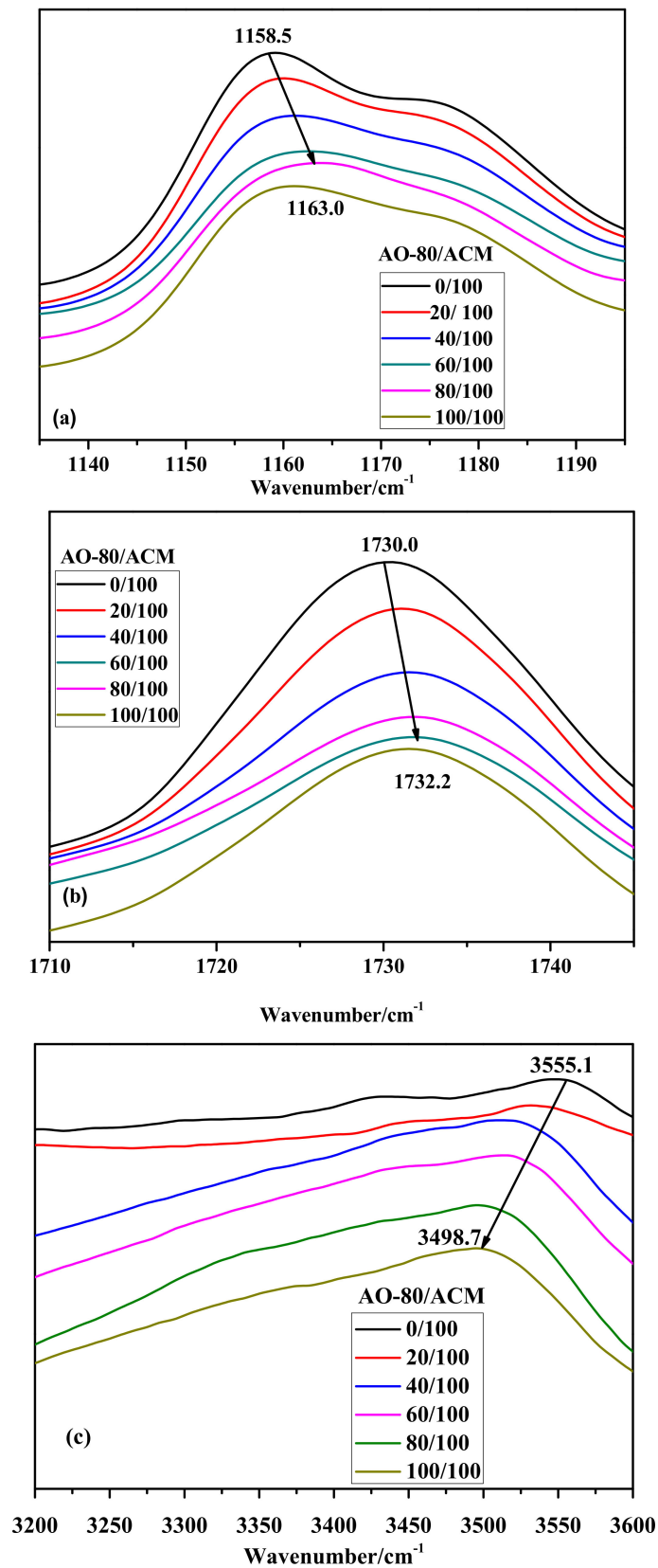


**Figure 3.** FT-IR spectra acquired at: (a) 1135 cm<sup>-1</sup> to 1195 cm<sup>-1</sup>; (b) 1710 cm<sup>-1</sup> to 1745 cm<sup>-1</sup>; and (c) 3200 cm<sup>-1</sup> to 3600 cm<sup>-1</sup> region for AO-80/ACM rubber composites.

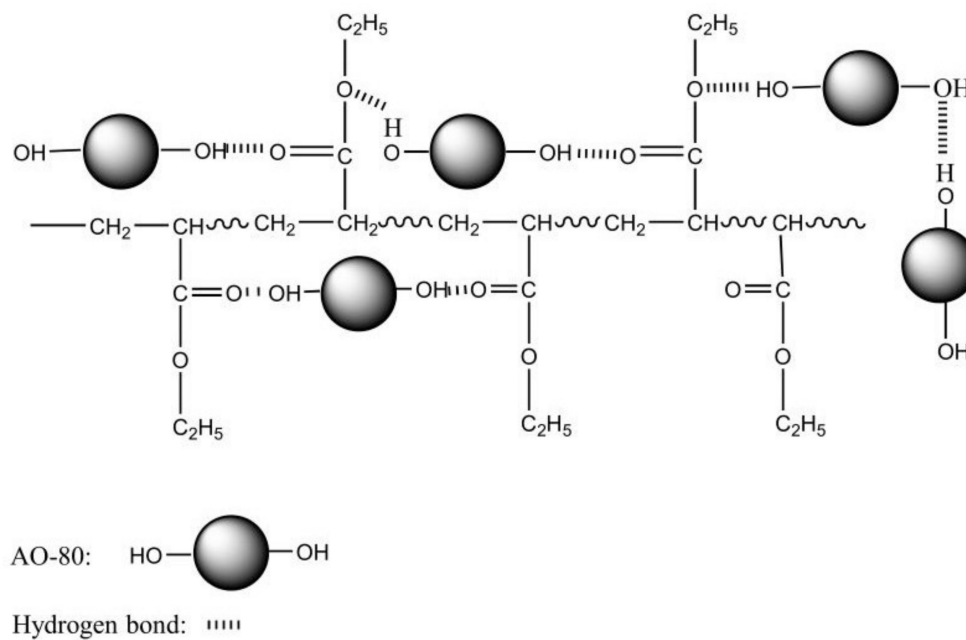


**Figure 4.** Possible hydrogen bond between AO-80 and ACM.

### 3.3. Static Mechanical Properties of AO-80/ACM Rubber Composites

The results of the tensile testing of neat ACM and AO-80/ACM rubber composites are shown in Figure 5 and the acquired data is summarized in Table 1. The elongation and tensile strength at break of the neat ACM were 210% and 1.47 MPa, respectively. All of the AO-80/ACM rubber composites with a content of AO-80 above forty phr had much longer elongation and higher tensile strength at break than ACM. This was because AO-80 had a reinforcement effect when AO-80 was added over 40 phr and the strength of hydrogen bonding among functional groups between ACM and AO-80 was improved when the AO-80 content was added increasingly.

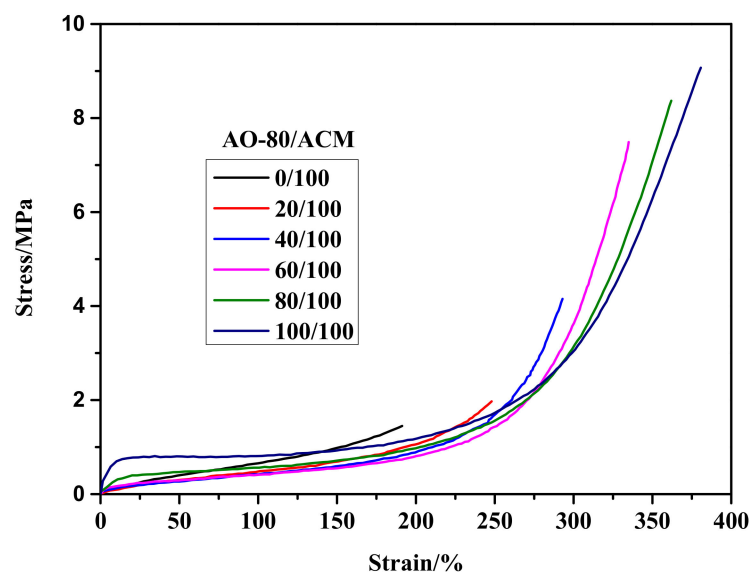


**Figure 5.** Stress-strain curves of ACM and AO-80/ACM rubber composites.

**Table 1.** Mechanical properties of AO-80/ACM rubber composites.

Properties	Loadings of AO-80/phr					
	0	20	40	60	80	100
Hardness (Shore A)	41 ± 0	48 ± 0	68 ± 0	78 ± 0	93 ± 0	95 ± 0
Tensile strength (MPa)	1.5 ± 0.2	1.9 ± 0.1	4.0 ± 0.2	7.7 ± 0.1	8.2 ± 0.1	9.2 ± 0.2
Elongation at break (%)	210 ± 9	248 ± 11	295 ± 12	336 ± 8	369 ± 8	377 ± 5

### 3.4. Shape-Memory Effect of AO-80/ACM Rubber Composite

Figure 6 depicts the 3D  $\varepsilon$ -T- $\sigma$  curves of various compositions for AO-80/ACM rubber composites. The results showed that the samples were generally further deformed because of loading during the cooling/fixing step after deformation, and the  $T_g$  of AO-80/ACM rubber composites increased with an increasing dosage of AO-80; in other words, the  $T_{trans}$  of AO-80/ACM rubber composites also increased with increasing AO-80. All samples exhibited excellent shape recovery, as shown in Figure 6. All the samples presented a high shape fixing ratio and recovery ratio when they were stretched to a given strain (100%).  $R_r$  and  $R_f$  were both above 99%. Figure 7 plots the 3D  $\varepsilon$ -T- $\sigma$  curves of five cycles for AO-80/ACM (40/100) rubber composite. The 3D  $\varepsilon$ -T- $\sigma$  curves of AO-80/ACM (40/100) rubber composites were similar with different cycles. Different cycles all showed high shape fixing and recovery rates. The results showed the repeatability of AO-80/ACM rubber composites as shape-memory materials were excellent. The excellent repeatability of AO-80/ACM rubber composites was due to good elasticity of samples. Figure 8 plots the 3D  $\varepsilon$ -T- $\sigma$  curves of different strains (deformation) for AO-80/ACM (60/100) rubber composite. All the diagrams show high shape fixing and recovery ratio when the given strains were 55%, 100%, and 130%.  $R_r$  reached above 99%, and  $R_f$  was above 99%. The results show that the range of deformation for the AO-80/ACM rubber composites as shape-memory materials is broad, which is due to high elongation at break of AO-80/ACM rubber composites. Figure 9 displays the  $R_r$ -T curves of AO-80/ACM rubber composites with various compositions. A significant portion of prestrain was recovered in all samples within the temperature range of  $T_{10}$ - $T_{90}$ . With increasing AO-80, the recovery temperature,  $T_{10}$  ( $R_r = 10\%$ ),  $T_{50}$  ( $R_r = 50\%$ ),  $T_{90}$  ( $R_r = 90\%$ ) increased, which was due to intermolecular interactions significantly hindering the slide of ACM chain and increasing the  $T_g$  ( $T_{trans}$ ) of AO-80/ACM rubber composites. Figures 6–9 show that AO-80/ACM rubber composites exhibit excellent shape-memory behavior.

The possible molecular mechanism of AO-80/ACM rubber composites is that AO-80/ACM rubber composites consist of molecular switches that are temperature-sensitive netpoints. The permanent shape in AO-80/ACM rubber composites was determined by netpoints that are cross-linked by the cross-linking agent. The temporary shape was fixed by the vitrification of AO-80/ACM rubber composites. Samples can be deformed to a temporary shape above  $T_{trans} + 20$  °C, and the shape can be fixed at  $T_{trans} - 20$  °C under stress. When heated above  $T_{trans} + 60$  °C without stress, the specimen recovered its original shape because of the netpoints.

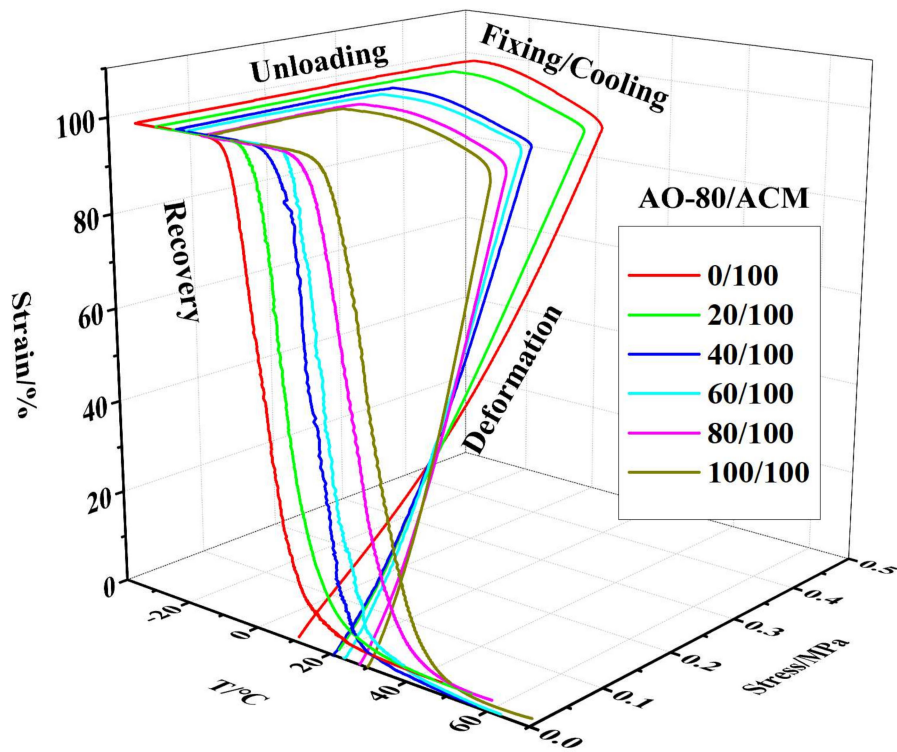


Figure 6. 3D  $\epsilon$ -T- $\sigma$  curve of various compositions for AO-80/ACM rubber composites.

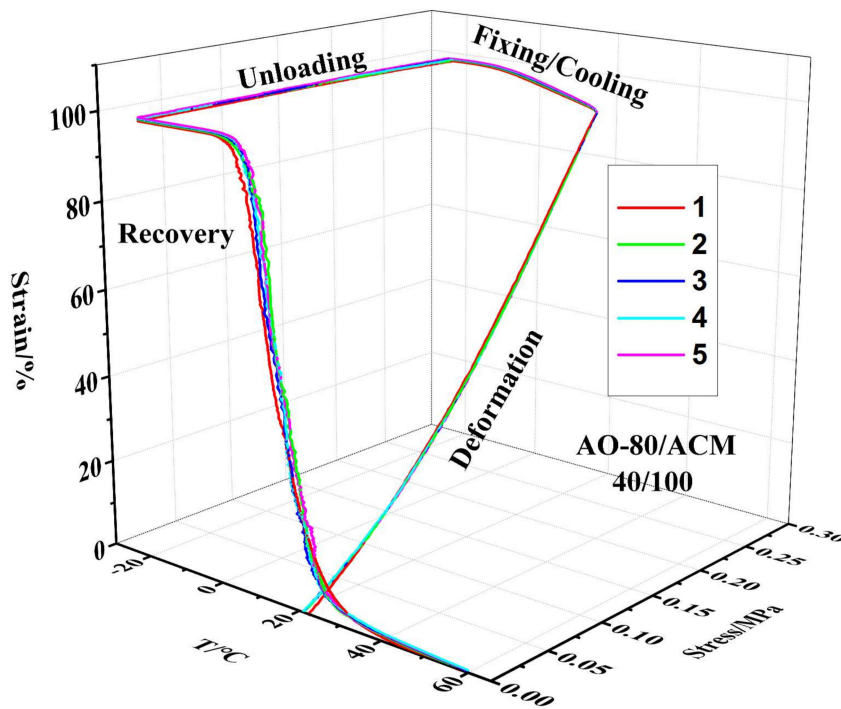


Figure 7. 3D  $\epsilon$ -T- $\sigma$  curve of five cycles for AO-80/ACM (40/100) rubber composite.

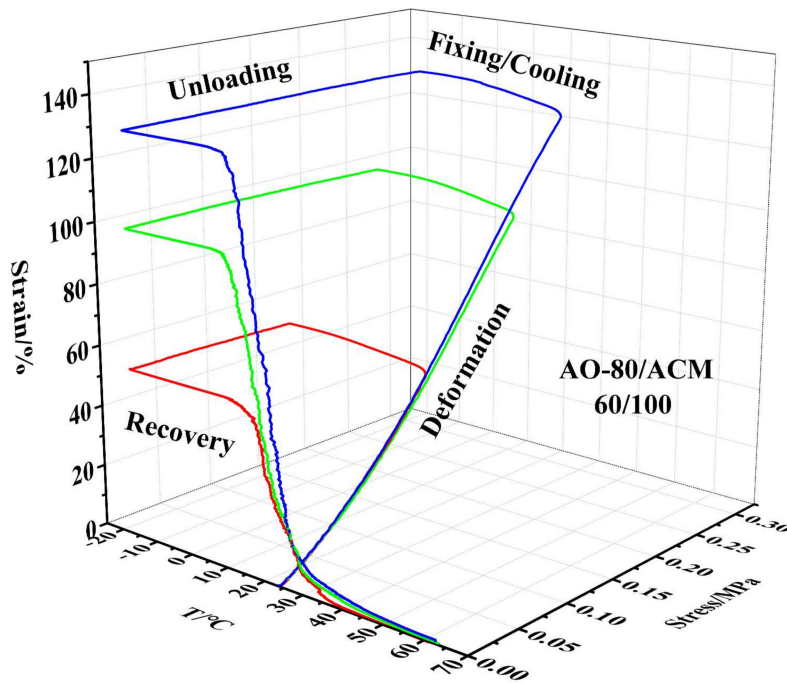


Figure 8. 3D  $\epsilon$ -T- $\sigma$  curves of different strains (deformation) for AO-80/ACM (60/100) rubber composite.

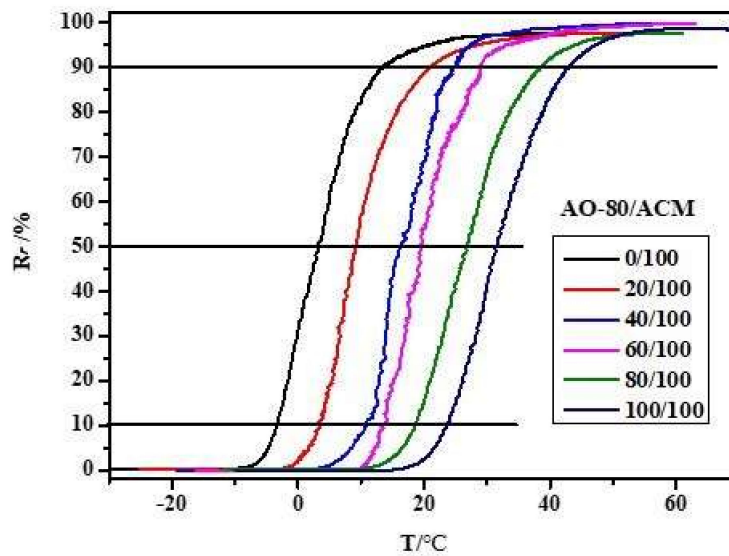
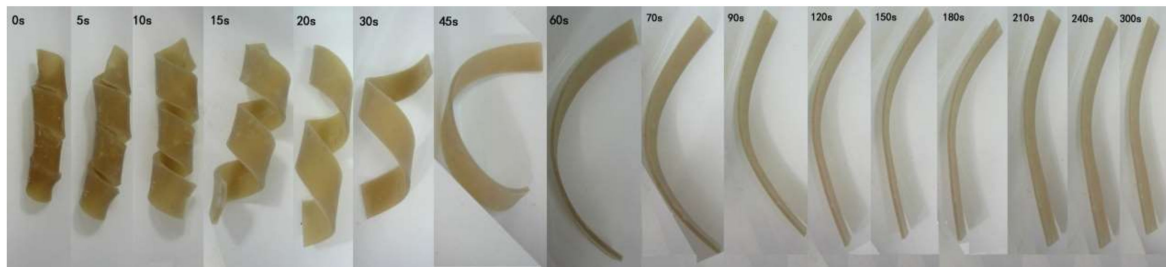


Figure 9.  $R_r$ -T curves of AO-80/ACM rubber composites.

Figure 10 shows the shape-memory recovery of AO-80/ACM (100/100) rubber composite. After placing the components in water at 20 °C, which is higher than  $T_g$ , they gradually recovered their original shape (Figure 10, t = 9 s–5 min). The results indicate that AO-80/ACM rubber composites exert shape-memory effects.



**Figure 10.** Shape recovery of AO-80/ACM rubber composites from a spiral-shaped temporary shape to stretched strip in water at 20 °C, which is higher than  $T_g$ .

### 3.5. Dynamic Mechanical Properties of AO-80/ACM Rubber Composites

Dynamic mechanical properties of AO-80/ACM rubber composites are shown in Figure 11. All curves have only one transition, and the curves moved toward higher temperatures with an increasing dosage of AO-80. The  $E'$  values of the AO-80/ACM rubber composites were similar in the glassy regions, whereas the  $E'$  values in the rubbery regions decreased with an increasing dosage of AO-80. This was because the  $E'$  values of AO-80 were similar to that of ACM matrix; therefore the  $E'$  values of AO-80/ACM rubber composites were similar in the glassy state. When AO-80/ACM rubber composites were in the rubbery state, temperature was higher than the  $T_g$  of AO-80 (40.9 °C) [44], the AO-80 acted as a plasticizer after becoming soft, therefore the  $E'$  values of AO-80/ACM rubber composites decreased. In AO-80/ACM rubber composites, all specimens showed a difference of approximately three orders of magnitude of AO-80/ACM rubber composites, which is responsible for the good recovery ratio and good shape fixity ratio for all specimens.

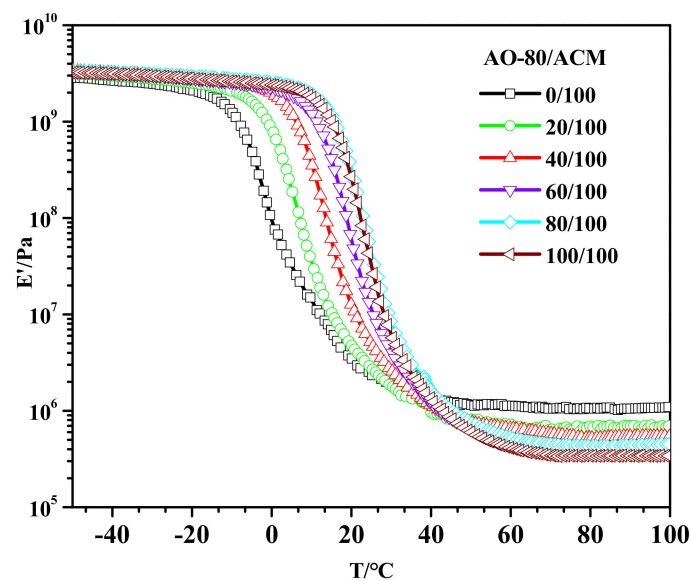


**Figure 11.**  $E'$ - $T$  curves of AO-80/ACM rubber composites.

## 4. Conclusions

In this work, AO-80/ACM rubber composites were prepared. AO-80 has been successfully used to tailor  $T_{trans}$  and  $T_g$  of AO-80/ACM rubber composites became higher with the increment in AO-80. The formation of hydrogen bonding between carbonyl and ether groups of ACM molecules and the -OH of AO-80 is responsible for the increase in  $T_g$ . Considering that  $T_{trans}$  of ACM and AO-80/ACM rubber composites was related to  $T_g$ , the  $T_{trans}$  of AO-80/ACM rubber composites shifted from  $-11$  °C to  $10$  °C when the dosage of AO-80 was added from zero phr to one hundred phr. In shape-memory experiments, the composites presented a shape-memory effect, and  $T_{10}$ ,  $T_{50}$ , and  $T_{90}$  increased with

$T_{trans}$ . Shape memory can be maintained at a wide deformation range and has good repeatability. All memory tests led to the conclusion that AO-80/ACM rubber composites feature excellent shape behavior.  $R_f$  and  $R_r$  of AO-80/ACM rubber composites were higher than 99% and 99%, respectively. The aforementioned approaches of tuning the transition temperature of developed composites can be potentially applied to other polymer systems.

**Author Contributions:** X.-y.Z. conceived and designed the experiments; S.-k.H. and S.C. performed the experiments; L.-q.Z. analyzed the data; M.-m.G. contributed reagents/materials/analysis tools; S.-k.H. wrote the paper.

**Funding:** This research was funded by [National Natural Science Foundation of China] grant number [51103006 and 51320105012].

**Acknowledgments:** We are thankful to Bao-chun Guo from the South China University of Technology and Wei-yu Cao from Beijing University of Chemical Technology for measurement of shape memory properties.

**Conflicts of Interest:** The authors declare no conflict of interest.

## References

1. Weiss, R.A.; Izzo, E.; Mandelbaum, S. New Design of Shape Memory Polymers: Mixtures of an Elastomeric Ionomer and Low Molar Mass Fatty Acids and Their Salts. *Macromolecules* **2008**, *41*, 2978–2980. [[CrossRef](#)]
2. Lendlein, A.; Kelch, S. Shape-Memory Polymers. *Angew. Chem. Int. Ed.* **2002**, *41*, 2034–2057. [[CrossRef](#)]
3. Sun, L.; Huang, W.M.; Ding, Z.; Zhao, Y.; Wang, C.C.; Purnawali, H.; Tang, C. Stimulus-responsive shape memory materials: A review. *Mater. Des.* **2012**, *33*, 577–640. [[CrossRef](#)]
4. Leng, J.S.; Lan, X.; Liu, Y.L.; Du, S.Y. Shape-memory polymers and their composites: Stimulus methods and applications. *Prog. Mater. Sci.* **2011**, *56*, 1077–1135. [[CrossRef](#)]
5. Lendlein, A.; Jiang, H.Y.; Jünger, O.; Langer, R. Light-induced shape-memory polymers. *Nature* **2005**, *434*, 879–882. [[CrossRef](#)] [[PubMed](#)]
6. Fabrizio, Q.; Loredana, S.; Anna, S.E. Shape memory epoxy foams for space applications. *Mater. Lett.* **2012**, *69*, 20–23. [[CrossRef](#)]
7. Lendlein, A.; Behl, M.; Hiebl, B.; Wischke, C. Shape-memory polymers as a technology platform for biomedical applications. *Expert Rev. Med. Devices* **2010**, *7*, 357–379. [[CrossRef](#)]
8. Liu, Y.P.; Gall, K.; Dunn, M.L.; Mcculsky, P. Thermomechanics of shape memory polymer nanocomposites. *Mech. Mater.* **2004**, *36*, 929–940. [[CrossRef](#)]
9. Squeo, E.A.; Quadrini, F. Shape memory epoxy foams by solid-state foaming. *Smart Mater. Struct.* **2010**, *19*, 533–536. [[CrossRef](#)]
10. Liu, Y.Y.; Han, C.M.; Tan, H.F.; Du, X.W. Thermal, mechanical and shape memory properties of shape memory epoxy resin. *Mater. Sci. Eng. A* **2010**, *527*, 2510–2514. [[CrossRef](#)]
11. Yang, B.; Huang, W.M.; Li, C.; Li, L. Effects of moisture on the thermomechanical properties of a polyurethane shape memory polymer. *Polymer* **2006**, *47*, 1348–1356. [[CrossRef](#)]
12. Huang, W.M.; Yang, B.; An, L.; Li, C. Water-driven programmable polyurethane shape memory polymer: Demonstration and mechanism. *Appl. Phys. Lett.* **2005**, *86*, 114105–114108. [[CrossRef](#)]
13. Lee, K.M.; Koerner, H.; Vaia, R.A.; Bunning, T.J.; White, T.J. Light-activated shape memory of glassy, Azobenzene liquid crystalline polymer networks. *Soft Matter* **2011**, *7*, 4318–4324. [[CrossRef](#)]
14. Koerner, H.; Price, G.; Pearce, N.A.; Alexander, M.; Vaia, R.A. Remotely actuated polymer nanocomposites-stress-recovery of carbon-nanotube-filled thermoplastic elastomers. *Nat. Mater.* **2004**, *3*, 115. [[CrossRef](#)] [[PubMed](#)]
15. Xiao, Y.Y.; Gong, X.L.; Kang, Y.; Jiang, Z.C.; Zhang, S.; Li, B.J. Light-, pH- and thermal-responsive hydrogels with the triple-shape memory effect. *Chem. Commun.* **2016**, *52*, 10609–10612. [[CrossRef](#)]
16. Yang, J.; Wen, H.; Zhuo, H.; Chen, S.; Ban, J. A new type of photo-thermo staged-responsive shape-memory polyurethanes network. *Polymers* **2017**, *9*, 287–297. [[CrossRef](#)]
17. Ji, F.L.; Zhu, Y.; Hu, J.L.; Liu, Y.; Yeung, L.Y.; Ye, G.D. Smart polymer fibers with shape memory effect. *Smart Mater. Struct.* **2006**, *15*, 1547. [[CrossRef](#)]

18. Du, F.P.; Ye, E.Z.; Yang, W.; Shen, T.H.; Tang, C.Y.; Xie, X.L.; Zhou, X.P.; Law, W.C. Electroactive shape memory polymer based on optimized multi-walled carbon nanotubes/polyvinyl alcohol nanocomposites. *Compos. Part B* **2015**, *68*, 170–175. [[CrossRef](#)]
19. Lu, H.B.; Liu, Y.J.; Gou, J.H.; Leng, J.S.; Du, S.Y. Synergistic effect of carbon nanofiber and carbon nanopaper on shape memory polymer composite. *Appl. Phys. Lett.* **2010**, *96*, 879. [[CrossRef](#)]
20. Lu, H.B.; Liu, Y.J.; Gou, J.H.; Leng, J.S.; Du, S.Y. Synergistic effect of carbon nanofiber and sub-micro filamentary nickel nanostrand on the shape memory polymer nanocomposite. *Smart Mater. Struct.* **2011**, *20*, 035017–035023. [[CrossRef](#)]
21. Lendlein, A.; Langer, R. Biodegradable, elastic shape-memory polymers for potential biomedical applications. *Science* **2002**, *296*, 1673–1676. [[CrossRef](#)] [[PubMed](#)]
22. Han, X.J.; Dong, Z.Q.; Fan, M.M.; Liu, Y.; Li, J.H.; Wang, Y.F.; Yuan, Q.J. pH-induced shape-memory polymers. *Macromol. Rapid Commun.* **2012**, *33*, 1055–1060. [[CrossRef](#)] [[PubMed](#)]
23. Meng, H.; Xiao, P.; Gu, J.; Wen, X.; Xu, J.; Zhao, C.; Zhang, J.; Chen, T. Self-healable macro-/microscopic shape memory hydrogels based on supramolecular interactions. *Chem. Commun.* **2014**, *50*, 12277–12280. [[CrossRef](#)] [[PubMed](#)]
24. Meng, H.; Zheng, J.; Wen, X.; Cai, Z.; Zhang, J.; Chen, T. Ph- and sugar-induced shape memory hydrogel based on reversible phenylboronic acid–diol ester bonds. *Macromol. Rapid Commun.* **2015**, *36*, 533–537. [[CrossRef](#)] [[PubMed](#)]
25. Yasin, A.; Li, H.Z.; Lu, Z.; Rehman, S.; Siddig, M.; Yang, H.Y. A shape memory hydrogel induced by the interactions between metal ions and phosphate. *Soft Matter* **2014**, *10*, 972. [[CrossRef](#)]
26. Ahn, S.; Deshmukh, P.; Kasi, R.M. Shape Memory Behavior of Side-Chain Liquid Crystalline Polymer Networks Triggered by Dual Transition Temperatures. *Macromolecules* **2010**, *43*, 7330–7340. [[CrossRef](#)]
27. Liu, C.D.; Chun, S.B.; Mather, P.T.; Zhang, L.; Haley, E.H.; Coughlin, E.B. Chemically Cross-Linked Polycyclooctene: Synthesis, Characterization, and Shape Memory Behavior. *Macromolecules* **2002**, *35*, 9868–9874. [[CrossRef](#)]
28. Liu, G.; Ding, X.; Cao, Y.; Zheng, Z.H.; Peng, Y.X. Shape Memory of Hydrogen-Bonded Polymer Network/Poly(ethylene glycol) Complexes. *Macromolecules* **2014**, *37*, 2228–2232. [[CrossRef](#)]
29. Cao, Y.P.; Guan, Y.; Du, J.; Luo, J.; Peng, Y.X.; Chan, A.S.C. Hydrogen-bonded polymer network-poly(ethylene glycol) complexes with shape memory effect. *J. Mater. Chem.* **2002**, *12*, 2957–2960. [[CrossRef](#)]
30. Liu, C.; Qin, H.; Mather, P.T. Review of progress in shape-memory polymers. *J. Mater. Chem.* **2007**, *17*, 1543–1558. [[CrossRef](#)]
31. Li, J.; Viveros, J.A.; Wrue, M.H.; Anthamatten, M. Shape-memory effects in polymer networks containing reversibly associating side-groups. *Adv. Mater.* **2007**, *19*, 2851–2855. [[CrossRef](#)]
32. Ware, T.; Hearon, K.; Lonnecker, A.; Wooley, K.L.; Maitland, D.J.; Voit, W. Triple-Shape Memory Polymers Based on Self-Complementary Hydrogen Bonding. *Macromolecules* **2012**, *45*, 1062. [[CrossRef](#)] [[PubMed](#)]
33. Chen, L.; Li, W.B.; Liu, Y.J.; Leng, J.S. Nanocomposites of epoxy-based shape memory polymer and thermally reduced graphite oxide: Mechanical, thermal and shape memory characterizations. *Compos. Part B* **2016**, *91*, 75–82. [[CrossRef](#)]
34. Lendlein, A.; Behl, M. Shape-memory polymers. *Mater. Today* **2007**, *10*, 20–28. [[CrossRef](#)]
35. Zhao, X.Y.; Cao, Y.J.; Zou, H.; Li, J.; Zhang, L.Q. Structure and Dynamic Properties of Nitrile- Butadiene Rubber /Hindered Phenol Composites. *J. Appl. Polym. Sci.* **2011**, *123*, 3696–3702. [[CrossRef](#)]
36. Zhao, X.Y.; Xiang, P.; Cao, Y.J.; Tian, M.; Fond, H.; Jin, R.G.; Zhang, L.Q. Nitrile butadiene rubber/hindered phenol nanocomposites with improved strength and high damping performance. *Polymer* **2007**, *48*, 6056–6063. [[CrossRef](#)]
37. Jiang, H.Y.; Kelch, S.; Lendlein, A. Polymers Move in Response to Light. *Adv. Mater.* **2006**, *18*, 1471–1475. [[CrossRef](#)]
38. Parameswaranpillai, J.; Ramanan, S.P.; Jose, S.; Siengchin, S.; Magueresse, A.; Janke, A.; Pionteck, J. Shape memory properties of epoxy/PPO-PEO-PPO triblock copolymer blends with tunable thermal transitions and mechanical characteristics. *Ind. Eng. Chem. Res.* **2017**, *56*, 14069–14077. [[CrossRef](#)]
39. Kumar, K.S.S.; Biju, R.; Nair, C.P.R. Progress in shape memory epoxy resins. *React. Funct. Polym.* **2013**, *73*, 421–430. [[CrossRef](#)]

40. Yu, R.; Yang, X.; Zhang, Y.; Zhao, X.; Wu, X.; Zhao, T.; Zhao, Y.; Huang, W. Three-dimensional printing of shape memory composites with epoxy-acrylate hybrid photopolymer. *ACS Appl. Mater. Interfaces* **2017**, *9*, 1820–1829. [[CrossRef](#)]
41. Wang, W.; Liu, D.; Liu, Y.; Leng, J.; Bhattacharyya, D. Electrical actuation properties of reduced graphene oxide paper/epoxy-based shape memory composites. *Compos. Sci. Technol.* **2015**, *106*, 20–24. [[CrossRef](#)]
42. Karger-Kocsis, J.; Kéki, S. Review of Progress in Shape Memory Epoxies and Their Composites. *Polymers* **2018**, *10*, 34. [[CrossRef](#)]
43. Xiao, D.L.; Zhao, X.Y.; Feng, Y.P.; Xiang, P.; Zhang, L.Q.; Wang, W.M. The structure and dynamic properties of thermoplastic polyurethane elastomer/hindered phenol hybrids. *J. Appl. Polym. Sci.* **2010**, *116*, 2143–2150. [[CrossRef](#)]
44. Ghobadi, E.; Heuchel, M.; Kratz, K.; Lendlein, A. Atomistic Simulation of the Shape-Memory Effect in Dry and Water Swollen Poly[(rac-lactide)-co-glycolide] and Copolyester Urethanes Thereof. *Macromol. Chem. Phys.* **2014**, *215*, 65–75. [[CrossRef](#)]
45. Ghobadi, E.; Heuchel, M.; Kratz, K.; Lendlein, A. Simulation of volumetric swelling of degradable poly[(rac-lactide)-co-glycolide] based polyesterurethanes containing different urethane-linkers. *J. Appl. Biomater. Funct. Mater.* **2013**, *10*, 293–301. [[CrossRef](#)] [[PubMed](#)]
46. Cao, Y.Y.; Mou, H.Y.; Shen, F.; Xu, H.Y.; Hu, G.H.; Wu, C.F. Hydrogenated nitrile butadiene rubber and hindered phenol composite. II. Characterization of hydrogen bonding. *Polym. Eng. Sci.* **2011**, *51*, 201–208. [[CrossRef](#)]
47. Wu, C.F. Microstructural development of a vitrified hindered phenol compound during thermal annealing. *Polymer* **2003**, *44*, 1697–1703. [[CrossRef](#)]
48. Zhao, X.Y.; Lu, Y.L.; Xiao, D.L.; Wu, S.Z.; Zhang, L.Q. Thermoplastic Ternary Hybrids of Polyurethane, Hindered Phenol and Hindered Amine with Selective Two-Phase Dispersion. *Macromol. Mater. Eng.* **2009**, *294*, 345–351. [[CrossRef](#)]



© 2018 by the authors. Licensee MDPI, Basel, Switzerland. This article is an open access article distributed under the terms and conditions of the Creative Commons Attribution (CC BY) license (<http://creativecommons.org/licenses/by/4.0/>).